IEEE Access
Multidisciplinary ⋮ Rapid Review ⋮ Open Access Journal

Received November 12, 2019, accepted December 29, 2019, date of publication January 6, 2020, date of current version January 15, 2020.

Digital Object Identifier 10.1109/ACCESS.2020.2964330

Inherent Interaction Analysis for Harmonic Oscillations in the Multi-Paralleled Grid-Connected Inverter System Using a Sum Type Criterion: Global Admittance (GA)

WU CAO[1,2], (Member, IEEE), SHUNYU WANG[1], HAOTIAN KANG[1], KANGLI LIU[1], (Member, IEEE), QINGSONG WANG[1], (Senior Member, IEEE), AND JIANFENG ZHAO[1]

[1]School of Electrical Engineering, Southeast University, Nanjing 210096, China
[2]Jiangsu Provincial Key Laboratory of Smart Grid Technology and Equipment, Nanjing 210096, China

Corresponding author: Shunyu Wang (shunyuwang@seu.edu.cn)

This work was supported in part by grants from the National Natural Science Foundation of China (51607037), Project funded by China Postdoctoral Science Foundation (2018M642138) and the Excellence Project Funds of Southeast University.

ABSTRACT With the extensive use of power electronics converters, harmonic oscillation issues in the multi-paralleled grid-connected inverter system have drawn much attention. Apart from the stability analysis using the impedance-based stability analysis method, the interaction analysis is aimed at revealing the changing process of the system state under the variation of some parameters such as the grid impendence, the number of grid-connected inverters and the control parameter of the inverter current control, etc. In this paper, after comparing the ratio type stability criterion and the sum type stability criterion, the interaction analysis using global admittance is presented in two frequency-domain dimensions. It shows that the harmonic instability depends on both the imaginary part of global admittance which determines the appearance of the resonance point and the real part of global admittance which reflects the property of such resonance point. The essence of this approach is to reveal the appearance of the resonance point and its influence on the system stability. The inherent changing rules of the resonance point are illustrated in the following typical occasions: different grid impendence, different number of grid-connected inverters and different control parameters of the current control loop. Finally, detailed simulations and experimental results validate the effectiveness of the proposed approach.

INDEX TERMS Harmonic oscillations, stability criterion, interaction analysis, global admittance, resonance point, point of common coupling (PCC).

I. INTRODUCTION

The grid-connected inverters are extensively applied in electrical grids ranging from renewable energy systems [1], [2], energy storage systems [3], [4] to electric railway systems [5], [6] to improve the capacity and reliability of systems. However, the large-scale adoption of inverters may cause interactive resonant current and resonance problems [7]–[9]. The interactions of the control system for inverters with each other and with passive components such as grid impendence may trigger small-signal oscillations [10], [11]. There are two typical small-signal stability issues which are low-frequency oscillations and the harmonic stability problem. The former one is mainly caused by the phase-locked loop (PLL) for grid-connected converters [12], [13] and the interactions among the slow outer power control loops [14], [15], while the latter one, resulting from the interactions among the fast inner current or voltage loops, may trigger system resonance at the harmonic frequency [16]. This paper only focuses on the harmonic instability issues. Thus, the low frequency oscillations can be neglected since the dynamics of outer control loops and PLL are designed much slower than the inner control loops [17], [18].

The associate editor coordinating the review of this manuscript and approving it for publication was Amin Hajizadeh.

There are two common analytical approaches for the harmonic stability problem: the eigenvalue-based analysis and the impedance-based analysis [19], [20]. The eigenvalue-based approach using the state-space modeling is normally implemented in the time-domain [21]. It can identify the system oscillation modes and the contributions for different state variables [22], [23]. However, due to the requirements of detailed information of each inverter and system parameters, this method cannot be readily used in some occasions [24], [25], and it requires a large amount of calculation [20].

By contrast, the system stability can be analyzed in the frequency-domain by the impedance-based analysis [17], [26], [27], originally used in the dc power system [28], [29] and then applied in the ac power system to analyze the interactions and stability issues [30], [31]. The grid-connected inverter system can be modeled as two subsystems, which are a current source in parallel with an output admittance, representing the inverter, and an ideal voltage source in series with a grid impedance, representing the grid [32]. Hence, the system stability can be obtained by using Nyquist stability criterion. Compared with the state-space model, the impedance-based approach no longer requires the formulation of system matrices [16] and detail information of system parameters [20].

In order to analyze the stability of the multi-paralleled grid-connected inverter system, the ratio type impendence-based stability analysis using minor loop gain (MLG) [18] or the global minor loop gain (GMLG) [33] are proposed. Apart from the ratio type approach, Liu et al. [34] proposes a sum type criterion, judging the system stability by checking whether the Nyquist plot of the sum of all units impedance encircles (0, 0) point. It can avoid the requirement of the information of right-half plane poles. Similarly, a global admittance-based stability criterion is proposed in [35] and the stability can be predicted based on the frequency characteristics of global admittance. In addition, the positive-net-damping stability criterion [36], [37], analyzing resonance instabilities in feedback systems, is also an effective way. These methods can analyze the harmonic stability problem conveniently. However, the interaction analysis, which is utilized to represents the changing process of the system state under different occasions has not been fully discussed. The stability analysis based on admittance characteristics is discussed briefly in [38], where the inherent principles have not been revealed.

In this paper, the comparison between the ratio type criterion and the sum type criterion is carried out and the advantages of the sum type criterion for the interaction analysis are presented. The interaction analysis using global admittance in two frequency-domain dimensions is implemented and it emphasizes the influence of the resonance point on system stability. By dividing the global admittance into two parts, which are the imaginary part and the real part, it reveals that the system stability is not only related to the system damping, but also determined by the resonance point. The appearance of the resonance point and its influence on system harmonic instability are revealed. In addition, by analyzing specific features of two parts, it reflects the impact of the variation of each component on system stability and finds the rules of the variation. Hence, it can not only provide more specific guidance for resonance suppression but is helpful to make stability-oriented design guidelines for inverters as well.

The system description and modeling are described in section II, where the ratio type criterion and the sum type criterion are presented briefly and the comparison between these two types of criteria is conducted. The interaction analysis based on global admittance is implemented in section III. Finally, time-domain simulations and experiments are performed in section IV in order to verify the validity of the proposed method.

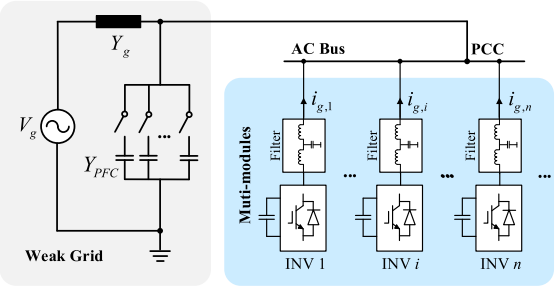

FIGURE 1. Typical single-phase multi-paralleled grid-connected inverter system.

II. STABILITY ANALYSIS METHODS FOR THE MULTI-PARALLELED GRID-CONNECTED INVERTER SYSTEM

A. SYSTEM DESCRIPTION AND MODELING

Fig. 1 illustrates a typical single-phase multi-paralleled grid-connected inverter system, where inverters are connected to the PCC, and a capacity-variable power factor correction (PFC) device is installed at the PCC. In such a system, the mutual interactions between the current control loops of inverters through the grid impedance may lead to stability problems. Again, this paper only focuses on the harmonic stability issues instead of the low-frequency oscillations. Only the inner current control loops are modeled, while impacts from the outer control loops and PLL can be neglected.

The current control loop of the ith inverter is shown in Fig. 2(a), where the PR controller is usually used as the current controller and the delay unit is usually caused by the computation and PWM. $Z_{f,i}$, $Z_{c,i}$, and $Z_{g,i}$ are the impedances for the inductor and the capacitor of the LCL filter. On the basis of Fig. 2 (a), the Norton equivalent model of the ith inverter can be drawn in Fig. 2 (b), which is shown as a controlled current source with a parallel parasitic admittance to the PCC. $I_{ref,i}$ and $I_{g,i}$ are the reference current and the output current for the ith inverter, $G_{c,i}$ represents the closed-loop gain of current loop and $Y_{oc,i}$ represents the output admittance seen from the PCC. The detailed derivation can be found in [39].

According to Fig. 2, the output admittance of the inverter can be derived as:

$$Y_{oc}(s) = \frac{Y_{LCLg}(s)}{1 + G_{PR}(s)\, G_d(s)\, Y_{LCLf}(s)} \tag{1}$$

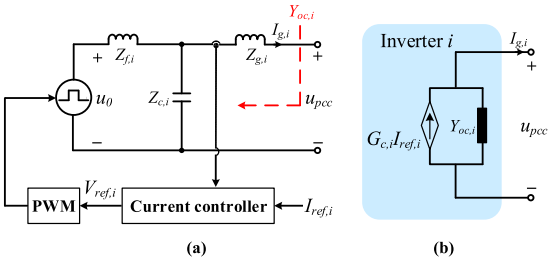

FIGURE 2. Illustration of the (a) current control loop and (b) Norton equivalent model of the *i*th inverter.

where $G_d(s)$ is the time delay in the digital control, $G_{PR}(s)$ is the PR controller, $Y_{LCLg}(s)$ and $Y_{LCLi}(s)$ are the frequency behavior of the *LCL* filter, which are expressed as:

$$G_d(s) = e^{-1.5T_s s} \approx \frac{(1.5T_s s)^2/12 - 1.5T_s s/2 + 1}{(1.5T_s s)^2/12 + 1.5T_s s/2 + 1} \tag{2}$$

$$Y_{LCLg}(s) = \frac{Z_f(s) + Z_c(s)}{Z_f(s)Z_g(s) + Z_g(s)Z_c(s) + Z_c(s)Z_f(s)} \tag{3}$$

$$Y_{LCLf}(s) = \frac{Z_c(s)}{Z_f(s)Z_g(s) + Z_g(s)Z_c(s) + Z_c(s)Z_f(s)} \tag{4}$$

$$G_{PR}(s) = K_p + \frac{K_i s}{s^2 + \omega_0^2} \tag{5}$$

where ω_0 is the fundamental frequency.

By substituting inverters with the Norton equivalent circuits, the multi-paralleled grid-connected inverter system shown in Fig.1 can be derived to the equivalent circuit shown in Fig.3.

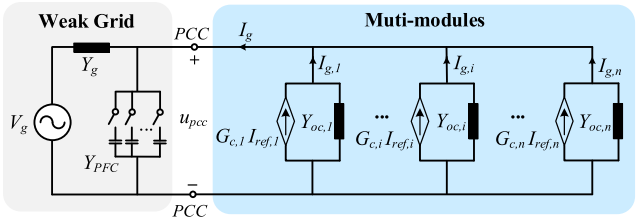

FIGURE 3. The equivalent circuit of multi-inverters grid-connected system.

B. RATIO TYPE STABILITY CRITERION

The ratio type criterion has been well discussed in many papers. There are two well-developed ratios: the minor loop gain (*MLG*) and the global minor loop gain (*GMLG*).

The *MLG* proposed in [18] is defined as the ratio between a single inverter output admittance and the combined admittance of grid, PFC device and all the other inverters. The *MLG* and the grid-injected current of the *i*th inverter are be expressed as

$$MLG_i = \frac{Y_{oc,i}}{Y_g + Y_{PFC} + \sum_{j=1,j\neq i}^{n} Y_{oc,j}} \tag{6}$$

$$I_{g,i} = \frac{1}{1 + MLG_i} G_{c,i} I_{ref,i} - \frac{MLG_i}{1 + MLG_i} \times \sum_{j=1,j\neq i}^{n} G_{c,i} I_{ref,j} - \frac{MLG_i}{1 + MLG_i} V_g Y_g \tag{7}$$

The *MLG* of single inverter reveals the complex coupling relationship between it and other inverters in the weak grid. On this basis, the *GMLG* proposed in [33] examines the interactions between all inverters and the weak grid from a global perspective. The *GMLG* of the whole system is defined as the ratio between the admittance of all inverters and the grid admittance combined the admittance of the PFC device, which can be expressed as

$$GMLG = \frac{\sum_{i=1}^{n} Y_{oc,i}}{Y_g + Y_{PFC}} \tag{8}$$

Thus, the total current from all inverters can be calculated and is derived as

$$I_g = \frac{1}{1 + GMLG} \sum_{i=1}^{n} \left(G_{c,i} I_{ref,i} - V_g Y_{oc,i} \frac{Y_g}{Y_g + Y_{PFC}} \right) \tag{9}$$

According to (7) and (9), the stability of the multi-paralleled grid-connected inverter system is determined by the number of right-half plane zeros (RHZ) of the denominator $1+MLG_i$ or $1+GMLG$. The classical Nyquist stability criterion can be applied and the system stability can be judged by determining whether the Nyquist curve of the MLG_i or *GMLG* encircle the critical point (-1, j0).

C. SUM TYPE STABILITY CRITERION

Compared to the ratio-based stability criterion, the sum type criterion is another effective approach. It is verified in [34] that two types of stability criterion are equivalent and both valid to evaluate the stability of some cascaded systems, while the sum type criterion is even more convenient in some special cases.

The global admittance-based criterion is proposed in [35], where the *GA* is defined as the summation of all the admittance in the grid-connected system, which can be expressed as:

$$Y_{total} = Y_g + Y_{PFC} + \sum_{i=1}^{n} Y_{oc,i} \tag{10}$$

The grid-injected current of *i*th inverter can be further expressed as:

$$I_{g,i} = G_{c,i} I_{ref,i} - \frac{Y_{oc,i}}{Y_{total}} G_{c,i} I_{ref,i} - \frac{Y_{oc,i}}{Y_{total}} \sum_{j=1,j\neq i}^{n} G_{c,j} I_{ref,j} - \frac{Y_{oc,i}}{Y_{total}} V_g Y_g \tag{11}$$

Similarly, the number of RHZ of the denominator Y_{total} determines the system stability and can be estimated by counting the number of times the trajectory of Y_{total} encircles the point (0, 0). Main features of two types of impendence stability criterion are given in Table 1.

D. COMPARISON BETWEEN DIFFERENT CRITERIA IN FREQUENCY DOMAIN

Table 2 summarizes main parameters for a typical power-electronics-based system with two grid-connected inverters.

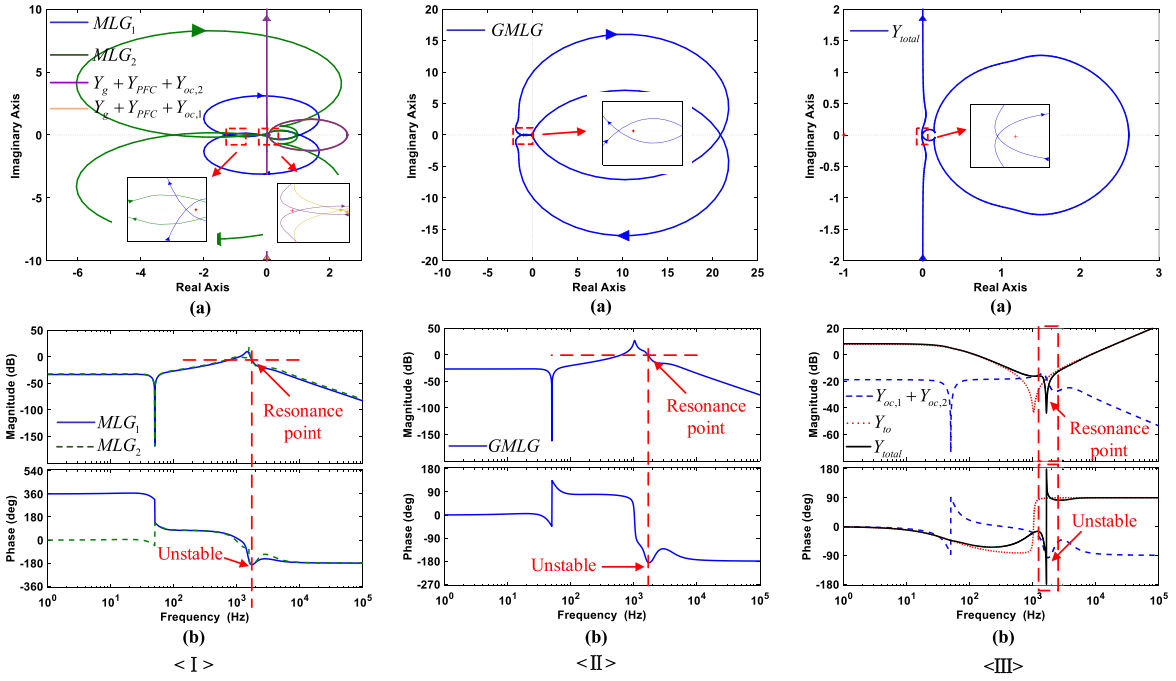

FIGURE 4. The (a) Nyquist plots and (b) Bode plots of different stability criteria when using < I > *MLG*, < II > *GMLG*, and < III > *GA*.

TABLE 1. Main features of two types of impedance stability criterion.

Stability criterion	Ratio type		Sum type
	MLG	GMLG	GA
Expression	$MLG_i = \frac{Y_{oc,i}}{Y_g + Y_{PFC} + \sum_{j=1,j\neq i}^{n} Y_{oc,j}}$	$GMLG = \frac{\sum_{i=1}^{n} Y_{oc,i}}{Y_g + Y_{PFC}}$	$Y_{total} = Y_g + Y_{PFC} + \sum_{i=1}^{n} Y_{oc,i}$
The determinant of system stability	1+*MLG*	1+*GMLG*	*GA*
The condition for system stable operation	The *MLG* satisfies Nyquist criterion	The *GMLG* satisfies Nyquist criterion	The Nyquist trajectory of *GA* doesn't encircle the point (0,0).

The Nyquist plots and Bode plots of MLG_i, *GMLG* and *GA* are drawn in Fig. 4, and the stability of the whole system can be assessed in the frequency domain with two types of stability criteria

It can be seen from Fig. 4 (a) of <I> that the denominator of MLG_i dose not have the right-half-plane zeros, thus there is no right-half plane poles (RHP) of MLG_i. Since there is also no right-half plane poles (RHP) *GMLG*, the Nyquist plots of each MLG_i and *GMLG* encircle (-1, j0), as shown in Fig. 4 (a) of <I> and <II>, indicating that the number of RHZ of 1+ MLG_i and 1+ *GMLG* derived in (7) and (9) are not zero. Hence, the system is unstable according to ratio type criterion. It can also be seen in Bode plots from Fig. 4 (b) of <I> and <II> that the phase of MLG_i and *GMLG* when magnitude equal 0dB are lower than -180°. Therefore, due to the negative phase margin of MLG_i and *GMLG*, the same conclusion can be obtained.

However, there are some differences when adopting sum type criterion. The unstable system can be seen from case III of Fig. 4 (a) of <III> as the Nyquist curve encircles the origin (0, 0), which means the number of RHZ of Y_{total} is not zero. It can be seen from Fig. 4 (b) of <III> that the sign of instability from Nyquist plot to Bode plot is a step change from -180° to 180 ° in the phase frequency response curve. This step change is corresponding to the crossing point of the Nyquist curve with the negative real axis. As the phase step change is an obvious and direct sign of an unstable system, the Bode plot of *GA* is more suitable for the stability judgement.

III. INTERACTION ANALYSIS USING GLOBAL ADMITTANCE IN TWO FREQUENCY-DOMAIN DIMENSIONS

A. DESCRIPTION OF THE PROPOSED METHOD

According to the definition of global admittance, the system can be regarded as a *RLC* resonant circuit. Based on

TABLE 2. Main parameters.

Parameters			Values
Inverter 1	*LCL*-filter	$L_{f,1}$	1.5 mH
		$R_{Lf,1}$	0.1 Ω
		$C_{f,1}$	4.7 μF
		$L_{g,1}$	1.8 mH
		$R_{Lg,1}$	0.2 Ω
	PR current controller	$K_{p,1}$	18
		$K_{i,1}$	3000
Inverter 2	*LCL*-filter	$L_{f,2}$	1.8 mH
		$R_{Lf,2}$	0.1 Ω
		$C_{f,2}$	3 μF
		$L_{g,2}$	1.3 mH
		$R_{Lg,2}$	0.2 Ω
	PR current controller	$K_{p,2}$	16
		$K_{i,2}$	3000
Switching frequency		f_s	10 kHz
DC-link voltage		V_{dc}	700 V
Grid		L_s	1.2 mH
		R_s	0.4 Ω
PFC device capacity		Y_{PFC}	20 μF

the global admittance-based stability criterion, the imaginary part of Y_{total} is zero at the intersection point of the Nyquist plot and real axis [35]. Therefore, such interaction point can be defined as the resonance point and the real part of the resonance point is defined as the resonance damping factor (RDF) R_d, which is able to reflect the system damping and is expressed as:

$$R_d = Y_{total}\,(j\omega)\,|_{\mathrm{Im}=0} \tag{12}$$

Therefore, the sign of R_d can also be applied to the stability judgment. If R_d is negative, the Nyquist plot would encircle the origin $(0, j0)$, which represents the system is unstable. By contrast, the positive value of R_d means that there is no encirclement around $(0, j0)$ and the system is therefore stable. Further, the system is more stable when R_d is larger.

In order to reveal the influence of resonance point and the changing rules under different occasions in detail, the interaction analysis using global admittance in two frequency-domain dimensions needs to be implemented. Dividing the global admittance into two dimensions which are the real part and the imaginary part, which can be expressed as:

$$\begin{aligned} Y_{total}\,(j\omega) &= \sum Y_{oc,i}\,(j\omega) + Y_{to}\,(j\omega) \\ &= \underbrace{\sum R_{oc,i}\,(j\omega) + R_{to}\,(j\omega)}_{R_d(j\omega)} \\ &\quad + \underbrace{\sum X_{oc,i}\,(j\omega) + X_{to}\,(j\omega)}_{X_d(j\omega)} \end{aligned} \tag{13}$$

where

$$Y_{to}\,(j\omega) = Y_g\,(j\omega) + Y_{PFC}\,(j\omega) \tag{14}$$

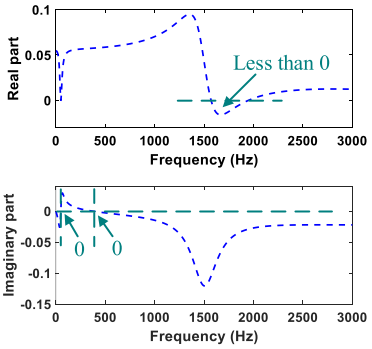

FIGURE 5. Output admittance characteristics of the grid-connected inverter.

$$R_{to}\,(j\omega) = R_g\,(j\omega) + R_{PFC}\,(j\omega) \tag{15}$$

$$X_{to}\,(j\omega) = X_g\,(j\omega) + X_{PFC}\,(j\omega) \tag{16}$$

where $R_d(j\omega)$ and $X_d(j\omega)$ are the real part and the imaginary part of $Y_{total}(j\omega)$. $R_{oc,i}(j\omega)$ and $X_{oc,i}(j\omega)$ are the real part and the imaginary part of $Y_{oc,i}(j\omega)$. $R_g(j\omega)$ and $X_g(j\omega)$ are the real part and the imaginary part of $Y_g(j\omega)$. $R_{PFC}(j\omega)$ and $X_{PFC}(j\omega)$ are the real part and the imaginary part of $Y_{PFC}(j\omega)$.

The global admittance has two properties which are the susceptance X_d and the conductance R_d, reflecting the appearance of the resonance point and the system state at the resonance point respectively. Therefore, the system is unstable if the R_d (*i.e.* the system damping) is negative when the corresponding X_d is zero (*i.e.* at the resonance point). The system is stable in the following three conditions:

1) There is no resonance point in the system, which means the X_d is positive or negative in the whole frequency range.
2) The R_d is larger than zero in the whole frequency range which means the system damping is always positive.
3) The system has negative damping bands and there are resonance points in the system, but those resonance points are not located in the negative damping bands. In other words, R_d is positive when the corresponding X_d is zero.

It is evident that X_d and R_d are both responsible for system harmonic instability. Thus, the interaction analysis in these two dimensions can reflect the influence of both the resonance point and the system damping, especially the former one. In addition, when parameters of each unit change, the variation rules of system characteristics including the variation of system damping and the location of the resonance point can be observed easily.

The interaction analysis using this method in an ideal grid without grid impendence is discussed as follows.

The parameters of the grid-connected inverter are the same as inverter 1 in Table 2. Hence, the frequency characteristics of the real part and the imaginary part of $Y_{oc}(s)$ can be obtained as shown in Fig. 5. The imaginary part of the output admittance of such LCL type inverter has two zero-crossing points in the low frequency band and it becomes less than zero when the real part has a negative value in a certain frequency band at the middle frequency band.

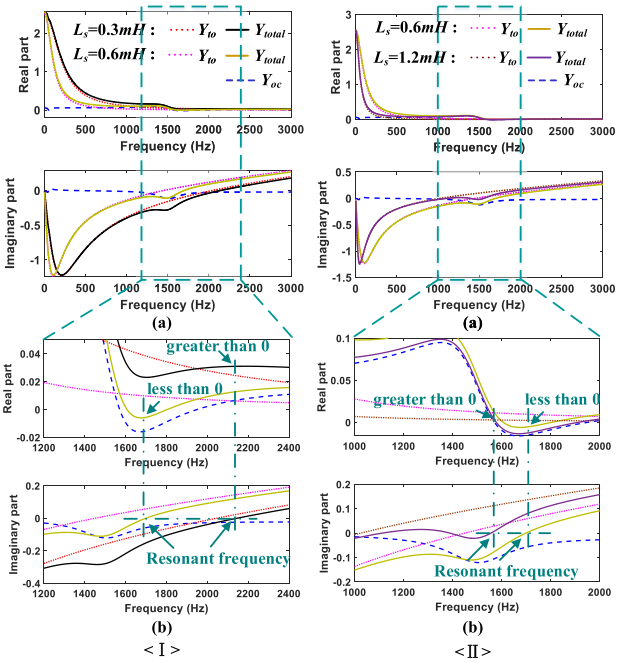

FIGURE 6. System admittance characteristics with different grid impedance. (a) Full view and (b) details around the resonance point of the comparison when grid impendence is <I> 0.3 mH and 0.6 mH and <II> 0.6 mH and 1.2 mH.

Therefore, in an ideal power grid without grid impendence, where the global admittance equals to the inverter output admittance, there is no resonance point located in the frequency band where the real part is negative, indicating that the system is stable. The interaction analysis under different occasions are discussed in the following section IV-B to section IV-E.

B. DIFFERENT GRID IMPEDANCE

Fig. 6 illustrates the characteristics of output admittance of the inverter 1, grid admittance and global admittance under different grid impedance conditions.

As can be seen in Fig. 6 <I>, when grid impedance is small (0.3mH), the imaginary part of global admittance has a zero-crossing point, indicating the appearance of the resonance point. However, due to the positive value of grid admittance, the real part of global admittance has no negative value. Therefore, the system is stable because of the positive damping of Y_{total} at the resonance point.

It is shown in Fig. 6 <I> (b) that the imaginary part of the grid admittance increases with grid impedance (0.6mH), resulting in the decrease of the resonance point frequency. As the real part of grid admittance declines, the real part of global admittance reaches to a negative value in a certain frequency band, which means that the system exhibits a negative damping characteristic in this frequency band. Thus, the frequency of the resonance point is located in the negative frequency band of the real part, indicating the system instability.

The imaginary part of grid admittance increases continuously with an increasing of grid impedance (1.2mH) as shown in Fig. 6 <II>, resulting in a further decrease of the frequency of the resonance point. The real part of grid admittance further reduces, and the real part of global admittance is closer to the counterpart of the inverter output admittance, meaning that the negative frequency band of the real part extends and the amplitude is lower. However, since the frequency of the resonance point is not located at the band where the real part is negative, the system is stable.

It should be noticed that there might be multiple zero-crossing points of the imaginary part of global admittance. For example, the curve of imaginary part in Fig. 6 <II> (b) (the solid purple line)when L_s equals to 1.2mH shows that there are two more zero-crossing points on the left side of the resonance point. The point where the value of the imaginary part changes from negative to positive is defined as the negative resonance point and the point where the value of the imaginary part changes from positive to negative is defined as the positive resonance point. It is clear that these two points are far from the negative damping zone of the real part, so the closest negative resonance point to such negative damping zone is the major resonance point which is around 1550Hz. Corresponding to the Nyquist criterion, these three points are interaction points of the Nyquist curve with the positive real axis and the closest point to the negative real axis determines the major characteristic. It should also be mentioned that similar to the Nyquist criterion, if there are multiple negative and positive resonance points in the negative damping zone, these two types of resonance point would cancel each other out and the last single negative resonance point the is the major resonance point.

C. DIFFERENT NUMBER OF GRID-CONNECTED INVERTERS

Stability analysis are carried out under different number of inverters, as shown in Fig. 7. The inverter parameters are same as the inverter 1 in Table 2.

Compared with only one inverter connected to the grid, when the number of inverters rises (three units), the absolute value of both the real part and imaginary part of output admittance of inverters increases. Therefore, the imaginary part of global admittance decreases, and consequently the resonance point frequency rises as shown in Fig. 7 <I> (b). In addition, the real part of the global admittance has a constant negative damping band range, but the amplitude is lower. Since the frequency of the resonance point rises and is located at the negative damping band of the real part, the system becomes unstable.

A similar trend can be seen in Fig. 7 <II> (b) when the number of inverters continues to increase (eight units). The imaginary part of global admittance continues to decrease, and the frequency of the resonance point continues to rise. Besides, the negative damping range of the real part is unchanged, but the absolute value of negative damping continues to increase. However, since the frequency of the resonance point continues to rise and is not located in the negative damping band of the real part, the system becomes stable from unstable.

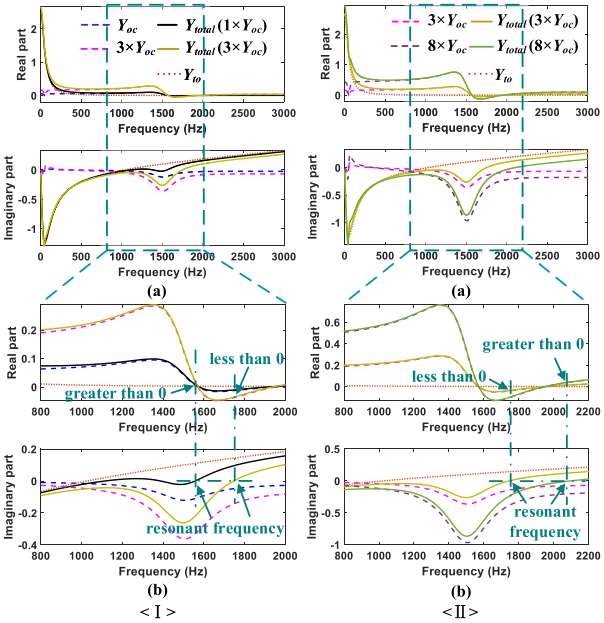

FIGURE 7. System admittance characteristics with different number of inverter. (a) Full view and (b) details around the resonance point of the comparison when the number of inverter is <I> one and three and <II> three and eight.

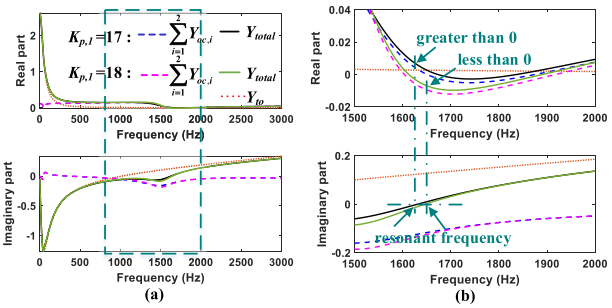

FIGURE 8. System admittance characteristics with different $K_{p,1}$: (a) Full view, (b) Details around the resonance point.

D. DIFFERENT PARAMETERS OF CURRENT CONTROL LOOP

In this occasion, there are two inverters with different parameters connected to the grid and parameters are shown in Table 2. The result of the comparison between different $K_{p,1}$, which are 17 and 18, of inverter 1 is depicted in Fig. 8.

Fig. 8 shows that with the increasing $K_{p,1}$, the imaginary part of inverter output admittance is slightly lower, resulting in a slight increase of resonant frequency. However, the real part of inverter output admittance decreases significantly, which means that the negative damping range is wider. The system becomes unstable as the resonance point is located in the negative damping range.

E. ADOPTION OF HARMONIC CONTROLLERS IN CURRENT CONTROL LOOP

It is true that the system may become unstable when employing multiple harmonic controllers [18]. The current controller

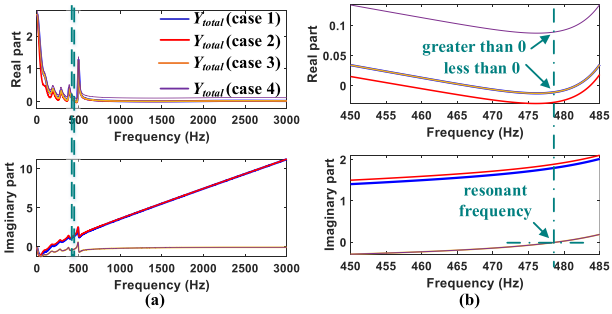

FIGURE 9. Global admittance with the adoption of harmonic controllers in current control loop: (a) Full view, (b) Details around the resonance point.

is changed as:

$$G_{PR}(s) = K_p + \frac{K_i s}{s^2 + \omega_0^2} + \sum_{h=3,5,7,9} \frac{K_{ih} s}{s^2 + (h\omega_0)^2} \quad (17)$$

where K_{ih} represents the gain of the harmonic controller, which is 2500 in this paper. Besides, K_p is reduced as 5 to guarantee the stable operation for the system without harmonic controllers and other inverter parameters are the same as the inverter 1 as shown in Table 2.

The system stability with three grid-connected inverters is analyzed in: (1) case 1, where the grid impedance is 1.2mH and the PFC is 600μF, (2) case 2, where the grid impedance is 1.8mH and the PFC is 600μF, (3) case 3, where the grid impedance is 1.2mH and there is no PFC device, and (4) case 4, where the grid impedance is 1.2mH and there is no PFC device but a resister load which is 10 Ω is connected to the PCC.

As shown in Fig. 9, the system is stable in case 1 and case 2 since the imaginary parts of Y_{total} are larger than zero when the real parts are negative, which means that there is no resonance point in the negative damping band. In case 3, there is a zero-crossing point of the imaginary part in the negative band of the real part, which implies the system is unstable under this occasion and the resonant frequency is around 478 Hz. In case 4, there is also a resonance point yet the real part is larger than zero at this point due to the contribution of the resistor load. Thus, the system is stable in this case.

Overall, the typical characteristics of the harmonic instability problem for the grid-connected inverter system from the physical circuit perspective can be summarized as follows:

1) The increase of the grid impedance will cause the decrease of the resonant frequency, and the range as well as the absolute value of the negative damping band of the real part of global admittance will increase.
2) An increase in the number of parallel inverters causes the frequency of the resonance point to rise. The range of the negative damping band of the real part of global admittance is unchanged, but the absolute value increases.
3) The grid-connected inverter system will become unstable within a certain range of grid impedance and the

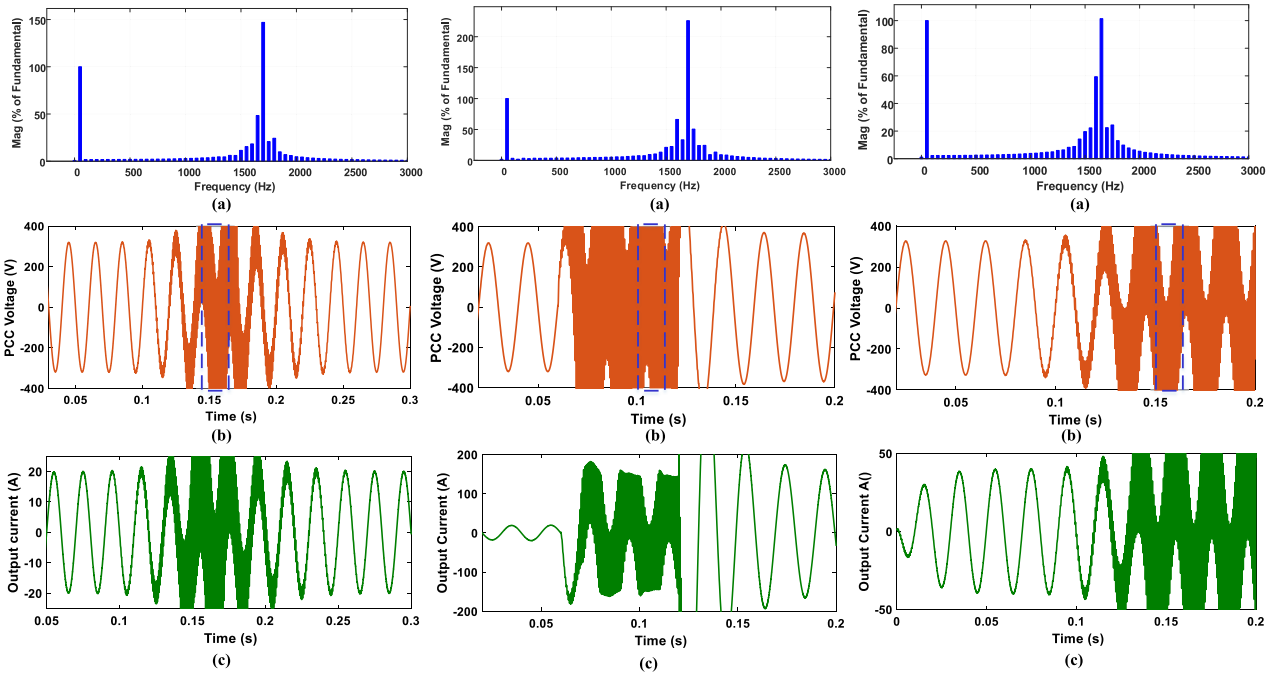

FIGURE 10. Simulation results. FFT analysis of PCC voltage at the resonant stage and the waveform of PCC voltage and output current of inverters under <I> different grid impendence, <II> different number of inverters and <III> different parameters of the current control loop.

number of inverters. The relationship between system stability and grid impedance as well as the number of paralleled units is complex instead of linear.

4) Increasing K_p may cause the system instability is mainly because that the negative damping range of inverter output admittance is wider so that the resonance point is more likely to be located in such range.
5) Harmonic controllers may result in the system instability at the controlled frequency. The variation of passive components has different impacts on system stability such as the appearance of the resonance point and the change on system damping.

The contribution of the proposed approach are summarized as follows:

1) By dividing the global admittance (GA) into the real part and the imaginary part, the system can be regarded as a *RLC* resonance circuit. Thus, the analysis of harmonic stability with the classical control theory (using the argument principle) is transformed to the analysis in the physical circuit.
2) The consideration of the resonance point indicates that the system negative damping is only the necessary condition for the harmonic instability, while the resonance point located in the negative damping zone is the necessary and sufficient condition. It means that the negative damping zone and the resonant point both should be considered in the harmonic instability problem analysis, while previous articles normally focus on the former one and the latter one has not been given fully consideration.

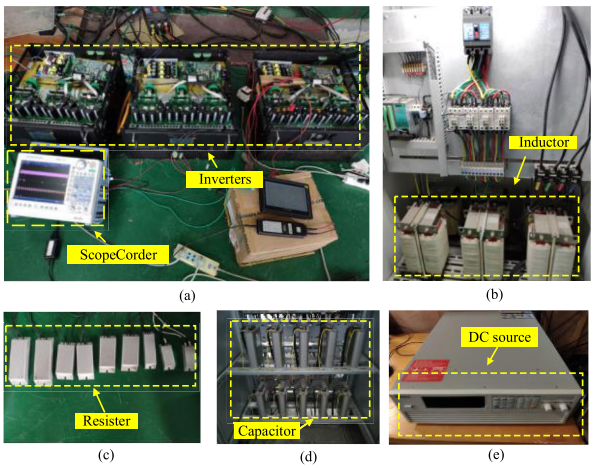

FIGURE 11. Experiment platform. (a) Three inverters and ScopeCorder-DL850E. (b) Inductor. (c) Resistor. (d) Capacitor. (e) DC source.

3) The resonance suppression and the design of the inverter can be considered from two perspectives which are improving the system damping and relocating the system resonance point to the secure frequency range. In addition, moving the location of the resonance point just need to vary the system reactive power, meaning that the oscillation suppression method can be cooperated with the reactive power compensation method.

IV. SIMULATION AND EXPERIMENT VERIFICATION

A. SIMULATION VERIFICATION

Fig. 10 <I> illustrates the simulation results for changes in grid impedance. The grid impedance is 0.3mH at first, and

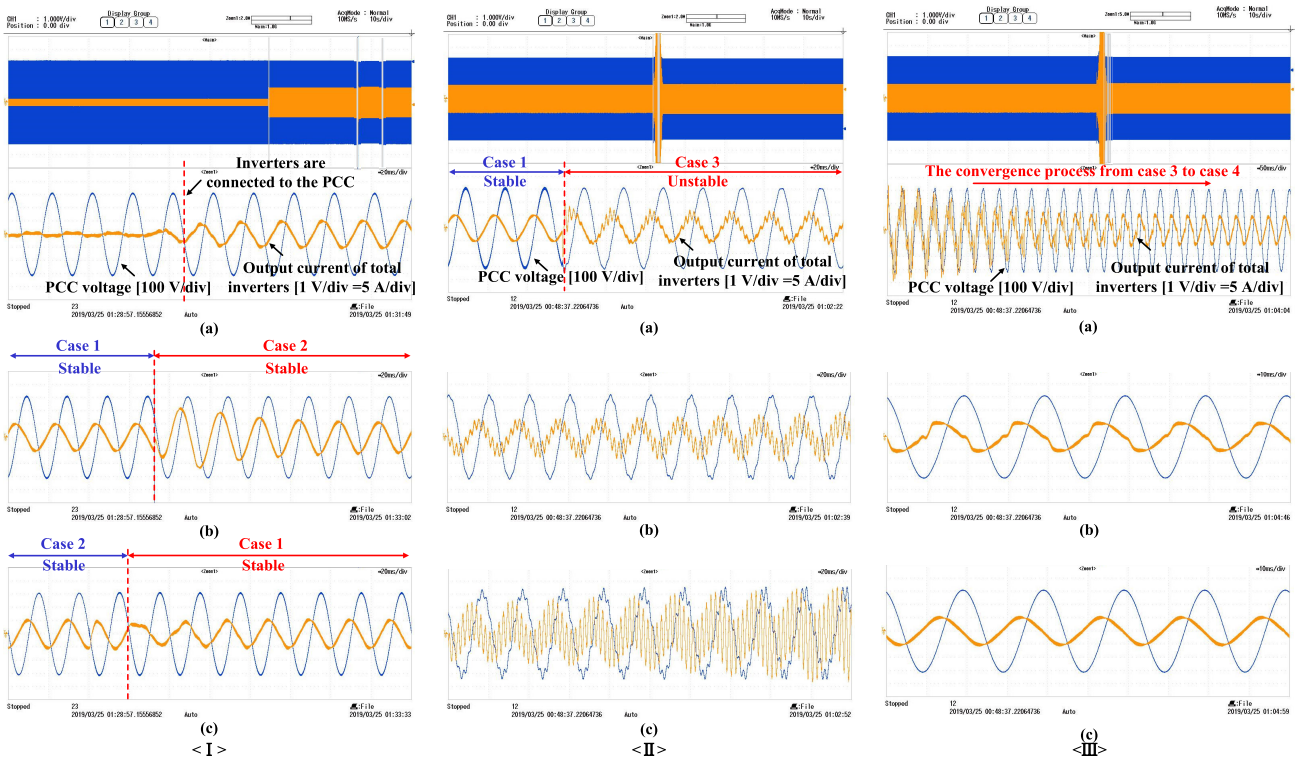

FIGURE 12. Experiment results between <I> case 1 and case 2, <II> case 1 and case 3 and <III> case 3 and case.

then varies to 0.6mH and 1.2mH at 0.06s and 0.17s respectively. The FFT analysis of the PCC voltage at the resonant stage is shown in Fig. 10 <I> (a). The PCC voltage and the output current of the grid-connected inverter are shown in Fig. 10 <I> (b) and (c), respectively.

It can be seen that the simulation results are correspond to the analysis results of Fig. 6. The system becomes unstable when the grid impedance increases, but the system re-stabilizes after the grid impedance continues to increase. In addition, when system is unstable, the resonant frequency, which is around 1700Hz, can be observed from Fig. 6. The same result can be obtained from Fig. 10 <I> (a).

Fig. 10 <II> shows the simulation results for different number of grid-connected inverters. One inverter is connected to the grid at first. Then, two inverters and the remaining five inverters are connected to the grid at 0.06 s and 0.12s, respectively. The FFT analysis of the PCC voltage at the resonant stage is shown in Fig. 10 <II> (a). The PCC voltage and the total output current of grid-connected inverters are shown in Fig. 10 <II> (b) and (c), respectively. The simulation results are correspond to the analysis from Fig. 7. With more paralleled inverters, the system become stable after destabilizing within a certain range.

Simulation results related to different K_p of inverter 1 are shown in Fig. 10 <III>. $K_{p,1}$ is set as 17 at first, and then is changed to 18 at 0.08s. It is apparent that the system become unstable when $K_{p,1}$ increases, which agrees with the analysis in Fig. 8.

B. EXPERIMENT VERIFICATION

Fig. 11 shows the experiment platform which consists of three grid-connected inverters. The inductor, the resistor and the capacitor are used to change the state of the passive components. The controller of inverters is based on DSP (TMS320F28335) and FPGA (EP3C5). It should be noticed that the source voltage is measured for synchronization in order to avoid the influence of PLL, and the DC source is utilized in the DC side of inverters in order to avoid the influence of the outer control loop. Fig. 12 <I> shows the PCC voltage and the output current of total inverters when inverters are connected to the PCC and the variation of system between case 1 and case 2. It is obvious that the system is stable in case 1, where three inverters are connected to the grid as shown in Fig. 12 <I> (a). In addition, the system remains stable when the grid impendence changes between 1.2mH and 1.8mH since there is no resonance point located at the negative band of the real part of global admittance, which agrees well with the analysis shown in Fig. 9. It should be mentioned that the full view of Fig. 12 <I> (b) and (c) is same with the one in Fig. 12 <I> (a) and the full view of Fig. 12 <II> and <III> are shown only once as well for the same reason.

Fig. 12 <II> depicts the PCC voltage and the output current of total inverters of the variation of system state between case 1 and case 3. It is evident, as shown in Fig. 12 <II> (a), that the system becomes unstable when the PFC is cut from the PCC, which is mainly due to the appearance of the

resonance point at the negative band of the real part of global admittance. The different stages of divergence are illustrated in Fig. 12 <II> (b) and (c), where the 9th harmonic current can be observed and it matches with the analysis in Fig. 9.

Fig. 12 <III> (a) illustrates the PCC voltage and the output current of total inverters of the variation of the system state in case 3 and case 4, where the system become stable when the resister load is connected to the PCC and the system damping is positive at the resonance point. The result is also accordance with the analysis in Fig. 9. One of stages of convergence and the stable state of case 4 are shown in Fig. 12 <III> (b) and (c) respectively.

In summary, the experimental results have verified the interaction analysis described in Section III-E, where four cases are discussed.

V. CONCLUSION

In this paper, the harmonic instability analysis and the interaction analysis for the multi-paralleled grid-connected inverter system have been studied. The comparison between the ratio type criterion and the sum type criterion has been carried out and it is found that the sum type criterion has more advantages for the interaction analysis. Further, the interaction analysis using global admittance in two frequency-domain dimensions has been conducted in this paper by separating the global admittance into the imaginary part and the real part. It shows that the harmonic instability depends not only on the real part, reflecting the system damping, but also on the imaginary part, which determines the resonance point. The appearance of the resonance point at the negative value band of the real part of global admittance is the essential factor for system instability while the grid impedance, the number of grid-connected inverters and the parameters of inverters can influence the location of the system resonance point. By analyzing specific features of two parts, the variation rules of system characteristics in different occasions have been summarized and it can provide specific guidance for future work such as resonance suppression and making stability-oriented design guidelines for the inverter. Finally, time-domain simulations and the experimental tests have been carried out. The results have confirmed the validity of the proposed approach.

REFERENCES

[1] F. Blaabjerg, Z. Chen, and S. Kjaer, "Power electronics as efficient interface in dispersed power generation systems," *IEEE Trans. Power Electron.*, vol. 19, no. 5, pp. 1184–1194, Sep. 2004.

[2] H. Hu, Q. Shi, Z. He, J. He, and S. Gao, "Potential harmonic resonance impacts of PV inverter filters on distribution systems," *IEEE Trans. Sustain. Energy*, vol. 6, no. 1, pp. 151–161, Jan. 2015.

[3] D. Bazargan, S. Filizadeh, and A. M. Gole, "Stability analysis of converter-connected battery energy storage systems in the grid," *IEEE Trans. Sustain. Energy*, vol. 5, no. 4, pp. 1204–1212, Oct. 2014.

[4] A. Ortega and F. Milano, "Generalized model of VSC-based energy storage systems for transient stability analysis," *IEEE Trans. Power Syst.*, vol. 31, no. 5, pp. 3369–3380, Sep. 2016.

[5] H. Tao, H. Hu, X. Wang, F. Blaabjerg, and Z. He, "Impedance-based harmonic instability assessment in a multiple electric trains and traction network interaction system," *IEEE Trans. Ind. Appl.*, vol. 54, no. 5, pp. 5083–5096, Sep. 2018.

[6] H. Hu, H. Tao, F. Blaabjerg, X. Wang, Z. He, and S. Gao, "Train-network interactions and stability evaluation in high-speed railways—Part I: Phenomena and modeling," *IEEE Trans. Power Electron.*, vol. 33, no. 6, pp. 4627–4642, Jun. 2018.

[7] Z. Shuai, D. Liu, J. Shen, C. Tu, Y. Cheng, and A. Luo, "Series and parallel resonance problem of wideband frequency harmonic and its elimination strategy," *IEEE Trans. Power Electron.*, vol. 29, no. 4, pp. 1941–1952, Apr. 2014.

[8] M. Lu, X. Wang, P. C. Loh, and F. Blaabjerg, "Resonance interaction of multiparallel grid-connected inverters with LCL filter," *IEEE Trans. Power Electron.*, vol. 32, no. 2, pp. 894–899, Feb. 2017.

[9] J. Kwon, X. Wang, F. Blaabjerg, C. L. Bak, V.-S. Sularea, and C. Busca, "Harmonic interaction analysis in a grid-connected converter using harmonic state-space (HSS) modeling," *IEEE Trans. Power Electron.*, vol. 32, no. 9, pp. 6823–6835, Sep. 2017.

[10] X. Wang, F. Blaabjerg, and P. C. Loh, "Grid-current-feedback active damping for LCL resonance in grid-connected voltage-source converters," *IEEE Trans. Power Electron.*, vol. 31, no. 1, pp. 213–223, Jan. 2016.

[11] D. Yang, X. Ruan, and H. Wu, "Impedance shaping of the grid-connected inverter with LCL filter to improve its adaptability to the weak grid condition," *IEEE Trans. Power Electron.*, vol. 29, no. 11, pp. 5795–5805, Nov. 2014.

[12] B. Wen, D. Dong, D. Boroyevich, R. Burgos, P. Mattavelli, and Z. Shen, "Impedance-based analysis of grid-synchronization stability for three-phase paralleled converters," *IEEE Trans. Power Electron.*, vol. 31, no. 1, pp. 26–38, Jan. 2016.

[13] X. Wang, L. Harnefors, and F. Blaabjerg, "Unified impedance model of grid-connected voltage-source converters," *IEEE Trans. Power Electron.*, vol. 33, no. 2, pp. 1775–1787, Feb. 2018.

[14] N. Bottrell, M. Prodanovic, and T. C. Green, "Dynamic stability of a microgrid with an active load," *IEEE Trans. Power Electron.*, vol. 28, no. 11, pp. 5107–5119, Nov. 2013.

[15] L. Harnefors, X. Wang, A. G. Yepes, and F. Blaabjerg, "Passivity-based stability assessment of grid-connected VSCs—An overview," *IEEE J. Emerg. Sel. Topics Power Electron.*, vol. 4, no. 1, pp. 116–125, Mar. 2016.

[16] X. Wang, F. Blaabjerg, and W. Wu, "Modeling and analysis of harmonic stability in an AC power-electronics-based power system," *IEEE Trans. Power Electron.*, vol. 29, no. 12, pp. 6421–6432, Dec. 2014.

[17] W. Cao, Y. Ma, and F. Wang, "Sequence-impedance-based harmonic stability analysis and controller parameter design of three-phase inverter-based multibus AC power systems," *IEEE Trans. Power Electron.*, vol. 32, no. 10, pp. 7674–7693, Oct. 2017.

[18] X. Wang, F. Blaabjerg, M. Liserre, Z. Chen, J. He, and Y. Li, "An active damper for stabilizing power-electronics-based AC systems," *IEEE Trans. Power Electron.*, vol. 29, no. 7, pp. 3318–3329, Jul. 2014.

[19] M. Amin and M. Molinas, "Small-signal stability assessment of power electronics based power systems: A discussion of impedance- and eigenvalue-based methods," *IEEE Trans. Ind. Appl.*, vol. 53, no. 5, pp. 5014–5030, Sep. 2017.

[20] X. Wang and F. Blaabjerg, "Harmonic stability in power electronic-based power systems: Concept, modeling, and analysis," *IEEE Trans. Smart Grid*, vol. 10, no. 3, pp. 2858–2870, May 2019, doi: 10.1109/TSG.2018.2812712.

[21] P. Kundur, *Power System Stability and Control*. New York, NY, USA: McGraw-Hill. 1994.

[22] Y. Wang, X. Wang, F. Blaabjerg, and Z. Chen, "Harmonic instability assessment using state-space modeling and participation analysis in inverter-fed power systems," *IEEE Trans. Ind. Electron.*, vol. 64, no. 1, pp. 806–816, Jan. 2017.

[23] Y. Wang, X. Wang, Z. Chen, and F. Blaabjerg, "Small-signal stability analysis of inverter-fed power systems using component connection method," *IEEE Trans. Smart Grid*, vol. 9, no. 5, pp. 5301–5310, Sep. 2018.

[24] N. Pogaku, M. Prodanovic, and T. C. Green, "Modeling, analysis and testing of autonomous operation of an inverter-based microgrid," *IEEE Trans. Power Electron.*, vol. 22, no. 2, pp. 613–625, Mar. 2007.

[25] W. Cao, Y. Ma, L. Yang, F. Wang, and L. M. Tolbert, "D-Q impedance based stability analysis and parameter design of three-phase inverter-based AC power systems," *IEEE Trans. Ind. Electron.*, vol. 64, no. 7, pp. 6017–6028, Jul. 2017.

[26] C. Yoon, H. Bai, R. N. Beres, X. Wang, C. L. Bak, and F. Blaabjerg, "Harmonic stability assessment for multiparalleled, grid-connected inverters," *IEEE Trans. Sustain. Energy*, vol. 7, no. 4, pp. 1388–1397, Oct. 2016.

[27] B. Wen, D. Boroyevich, R. Burgos, P. Mattavelli, and Z. Shen, "Inverse Nyquist stability criterion for grid-tied inverters," *IEEE Trans. Power Electron.*, vol. 32, no. 2, pp. 1548–1556, Feb. 2017.
[28] R. D. Middlebrook, "Input filter considerations in design and application of switching regulators," in *Proc. IEEE IAS Annu. Meeting*, Jan. 1976, pp. 366–382.
[29] X. Feng, J. Liu, and F. Lee, "Impedance specifications for stable DC distributed power systems," *IEEE Trans. Power Electron.*, vol. 17, no. 2, pp. 157–162, Mar. 2002.
[30] R. Turner, S. Walton, and R. Duke, "A case study on the application of the Nyquist stability criterion as applied to interconnected loads and sources on grids," *IEEE Trans. Ind. Electron.*, vol. 60, no. 7, pp. 2740–2749, Jul. 2013.
[31] Z. Liu, J. Liu, W. Bao, and Y. Zhao, "Infinity-norm of impedance-based stability criterion for three-phase AC distributed power systems with constant power loads," *IEEE Trans. Power Electron.*, vol. 30, no. 6, pp. 3030–3043, Jun. 2015.
[32] J. Sun, "Impedance-based stability criterion for grid-connected inverters," *IEEE Trans. Power Electron.*, vol. 26, no. 11, pp. 3075–3078, Nov. 2011.
[33] Q. Ye, R. Mo, Y. Shi, and H. Li, "A unified impedance-based stability criterion (UIBSC) for paralleled grid-tied inverters using global minor loop gain (GMLG)," in *Proc. IEEE Energy Convers. Congr. Exposit. (ECCE)*, Sep. 2015, pp. 5816–5821.
[34] F. Liu, J. Liu, H. Zhang, and D. Xue, "Stability issues of $Z + Z$ type cascade system in hybrid energy storage system (HESS)," *IEEE Trans. Power Electron.*, vol. 29, no. 11, pp. 5846–5859, Nov. 2014.
[35] W. Cao, K. Liu, S. Wang, H. Kang, D. Fan, and J. Zhao, "Harmonic stability analysis for multi-parallel inverter-based grid-connected renewable power system using global admittance," *Energies*, vol. 12, no. 14, p. 2687, Jul. 2019.
[36] L. Harnefors, "Proof and application of the positive-net-damping stability criterion," *IEEE Trans. Power Syst.*, vol. 26, no. 1, pp. 481–482, Feb. 2011.
[37] L. Sainz, M. Cheah-Mane, L. Monjo, J. Liang, and O. Gomis-Bellmunt, "Positive-net-damping stability criterion in grid-connected VSC systems," *IEEE J. Emerg. Sel. Topics Power Electron.*, vol. 5, no. 4, pp. 1499–1512, Dec. 2017.
[38] Y. Wang, S. Liu, J. Liu, H. Mei, and L. Chen, "Resonance mechanism analysis of the power system involving distributed grid-connected inverters," *Proc. CSEE*, vol. 38, no. 9, pp. 2693–2706, May 2018.
[39] X. Wang, F. Blaabjerg, and P. C. Loh, "Proportional derivative based stabilizing control of paralleled grid converters with cables in renwable power plants," in *Proc. IEEE Energy Convers. Congr. Expo. (ECCE)*, Sep. 2014, pp. 4917–4924.

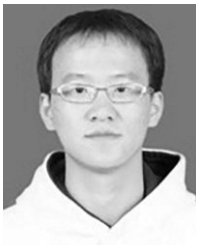

WU CAO (Member, IEEE) received the B.S., M.S., and Ph.D. degrees in electrical engineering from Southeast University, Nanjing, China, in 2007, 2011, and 2015, respectively. In 2016, he joined Southeast University, where he is currently a Lecturer with the School of Electrical Engineering. His research interests include the stability analysis and control of parallel-connected inverters, harmonic current suppression, and reactive power compensation.

SHUNYU WANG received the B.S. degree in electrical engineering and automation from China Agricultural University, Beijing, China, in 2017. He is currently pursuing the M.S. degree in electrical engineering with Southeast University, Nanjing, China. His research interests include the control strategy and stability analysis for renewable energy systems.

HAOTIAN KANG received the B.S. degree in electrical engineering from Hangzhou Dianzi University, Hangzhou, China, in 2017. He is currently pursuing the M.S. degree in electrical engineering with Southeast University, Nanjing, China. His research interests include harmonic current suppression, stability analysis and control of parallel-connected inverters, and power electronics for distributed generations.

KANGLI LIU (Member, IEEE) received the B.S. degree in electrical engineering and automation from the China University of Mining and Technology, Xuzhou, China, in 2011, and the M.S. and Ph.D. degrees in electrical engineering from Southeast University, Nanjing, China, in 2014 and 2017, respectively. Since January 2018, he has been a Postdoctoral Research Fellow with the School of Electrical Engineering, Southeast University. His research interests include harmonic current suppression, reactive power compensation, as well as stability analysis and control strategy for the parallel grid-connected inverters system.

QINGSONG WANG (Senior Member, IEEE) received the B.Sc. and M.Sc. degrees from the Department of Electrical Engineering, Zhejiang University, Hangzhou, China, in 2004 and 2007, respectively, and the Ph.D. degree from the School of Electrical Engineering, Southeast University, Nanjing, China, in 2016.

From November 2015 to November 2016, he was a joint Ph.D. student with the Department of Energy Technology, Aalborg University, Aalborg, Denmark, where he focused on electric springs. From July 2004 to July 2005, he was an Engineer at Shihlin Electronic & Engineering Company, Ltd., Suzhou, China. From July 2007 to August 2011, he was an Engineer with the Global Development Center of Philips Lighting Electronics, Shanghai, China. In October 2010, he was promoted to be a Senior Engineer. From August 2011 to September 2013, he was a Lecturer with the PLA University of Science and Technology, Nanjing, China. Since 2017, he has been with Southeast University, where he is currently a Lecturer with the School of Electrical Engineering. His research interest is focused in the areas of control and applications of power electronics to power systems.

JIANFENG ZHAO received the B.S. degree in electrical engineering from the Huainan Mining Institute, Anhui, China, in 1995, the M.S. degree in automation from the Nanjing University of Aeronautics and Astronautics, Nanjing, China, in 1998, and the Ph.D. degree in electrical engineering from Southeast University, Nanjing, in 2001.

In 2001, he joined the Faculty of the School of Electrical Engineering, Southeast University, where he has been a Professor, since 2008. He has been teaching and researching in the field of high-power electronics and has been serving as the Dean of the School of Electrical Engineering, Southeast University, since 2014. He has authored more than 100 technical papers. He currently holds 50 Chinese patents and two US patents. His main research interests are utility applications of power electronics in smart grids, such as solid-state transformers, active filters for power conditioning, flexible AC transmission system devices, multilevel ac motor drivers, and efficient energy utilization.